catalysts

MDPI

Communication

The Effects of the Crystalline Phase of Zirconia on C–O Activation and C–C Coupling in Converting Syngas into Aromatics

Sheng Wang, Yue Fang, Zhen Huang *, Hualong Xu and Wei Shen *

Department of Chemistry, Shanghai Key Laboratory of Molecular Catalysis and Innovative Materials Laboratory of Advanced Materials, Collaborative Innovation Center of Chemistry for Energy Materials, Fudan University, Shanghai 200433, China; swang14@fudan.edu.cn (S.W.); yfang17@fudan.edu.cn (Y.F.); shuhl@fudan.edu.cn (H.X.)

* Correspondence: huangzhen@fudan.edu.cn (Z.H.); wshen@fudan.edu.cn (W.S.); Tel.: +86-021-3124-2401 (W.S.)

Received: 16 January 2020; Accepted: 19 February 2020; Published: 21 February 2020

Abstract: Zirconia has recently been used as an efficient catalyst in the conversion of syngas. The crystalline phases of ZrO_2 in ZrO_2/HZSM-5 bi-functional catalysts have important effects on C–O activation and C–C coupling in converting syngas into aromatics and been investigated in this work. Monoclinic ZrO_2 (*m*-ZrO_2) and tetragonal ZrO_2 (*t*-ZrO_2) were synthesized by hydrothermal and chemical precipitation methods, respectively. The results of *in situ* diffuse reflection infrared Fourier transform spectroscopy (DRIFTs) revealed that there were more active hydroxyl groups existing on the surface of *m*-ZrO_2, and CO temperature programmed desorption (CO-TPD) results indicated that the CO adsorption capacity of *m*-ZrO_2 was higher than that of *t*-ZrO_2, which can facilitate the C–O activation of *m*-ZrO_2 for syngas conversion compared to that of *t*-ZrO_2. And the CO conversion on the *m*-ZrO_2 catalyst was about 50% more than that on the *t*-ZrO_2 catalyst. ^{31}P and ^{13}C magic angle spinning nuclear magnetic resonance (MAS NMR) analysis revealed a higher acid and base density of *m*-ZrO_2 than that of *t*-ZrO_2, which enhanced the C–C coupling. The selectivity to CH_4 on the *m*-ZrO_2 catalyst was about 1/5 of that on the *t*-ZrO_2 catalyst in syngas conversion. The selectivity to C_{2+} hydrocarbons over *m*-ZrO_2 or *t*-ZrO_2 as well as the proximity of the ZrO_2 sample and HZSM-5 greatly affected the further aromatization in converting syngas into aromatics.

Keywords: zirconia crystalline phase; syngas; aromatics; C–O activation; C–C coupling

1. Introduction

With declining petroleum resources, the efficient use of carbon-containing resources has received widespread interest in recent years [1]. The conversion of syngas is a promising route to obtain high value chemicals from non-petroleum resources due to the wide variety of sources of syngas [2]. Considerable efforts have been made in the conversion of syngas to a range of hydrocarbons such as lower olefins, gasoline, diesel, and aromatics [3–6]. Syngas to hydrocarbons reaction was firstly achieved in 1923, known as the Fischer-Tropsch synthesis (FTS). According to the mechanism of FTS, CH_2 intermediates are generally considered as polymerizable monomers, and products with different carbon chain lengths are formed on the catalyst surface via C–C coupling reactions, followed by hydrogenation or dehydrogenation [2]. However, the distribution of products follows the Anderson-Schulz-Flory (ASF) model, according to which the production of light olefins and paraffins for C_2–C_4 hydrocarbons is limited to about 58% [7]. Recently, bi-functional catalysts have been developed by combining metal oxides with zeolites (OX-ZEO), and high selectivity of light olefins and aromatics has been achieved, which has broken through the limitations of ASF distribution in FTS [8–17]. OX-ZEO catalysts

composed of oxides ($ZnCrO_x$) and zeolite (ZSM-5) were developed by physical mixing, which achieved a selectivity of 74% in direct converting syngas into aromatics [10]. Meanwhile, ZrO_2-based oxides have shown a decent catalytic activity in syngas conversion. An 80% selectivity of aromatics with 20% CO conversion was achieved by a bi-functional catalyst composed of Zn-ZrO_2 and HZSM-5 [11]. Mo-doped ZrO_2 has also been adopted, and exhibited a 76% selectivity to aromatics [14]. It is worth noting that the ZrO_2 possessed tetragonal crystalline phase with a small amount of monoclinic phase in these two catalysts. Others showed that 62% selectivity to aromatics with 12% CO conversion in the direct conversion of syngas can be achieved over nano-sized *t*-ZrO_2 and HZSM-5 bifunctional catalyst [15]. However, the different crystalline phases of ZrO_2 might affect its catalytic performance on this reaction, which still need to be investigated.

Due to the different coordination environments of zirconium and oxygen, the surface properties of *m*-ZrO_2 and *t*-ZrO_2 are different [18], which affect the C–O activation and C–C coupling in the reactions. The crystalline phase of ZrO_2 can be controlled by the synthesis method. Different crystalline phases of ZrO_2 have diverse catalytic activities in many reactions [19–27]. In the conversion of syngas to isobutane, *m*-ZrO_2 with strong basicity performed higher reaction rate and selectivity to isobutene [24]. In the hydrogenation of CO_2 to methanol, Cu/*t*-ZrO_2 catalyst showed a higher turnover frequency due to the stronger interaction between Cu and *t*-ZrO_2 as well as the higher ratio of H_2/CO_2 on the surface [25]. A similar effect is found in CO hydrogenation to methanol and higher alcohols, where the crystal phase of ZrO_2 could affect the activity of the catalysts as well as the product selectivity [26]. Therefore, the crystalline phase of ZrO_2 plays a very important role in the C–O activation and C–C coupling reactions in the conversion of syngas to aromatics.

As mentioned above, ZrO_2-based oxides and HZSM-5 bifunctional catalysts have shown good selectivity and stability in converting syngas into aromatics. To the best of our knowledge, there is no research on the effects of the crystalline phases of ZrO_2 on converting syngas into aromatics and the crystalline phases of ZrO_2 could play a very important role in the C–O activation and C–C coupling. We believe that such research is of great value to further optimize the ZrO_2-based bifunctional catalysts. In this work, we prepared ZrO_2 samples with monoclinic and tetragonal crystalline phases. Then, the surface properties of these ZrO_2 materials were investigated by CO-TPD, *in situ* DRIFTs, and $^{31}P/^{13}C$ MAS NMR. The effects of the crystalline phases of ZrO_2 on C–O activation and C–C coupling in converting syngas into aromatics have been evaluated.

2. Results and Discussion

2.1. Characterization of ZrO_2 Samples

2.1.1. Texture Properties of the Crystalline Phase of ZrO_2 Samples

ZrO_2 samples with different crystalline phase were synthesized by hydrothermal and chemical precipitation methods, respectively. X-ray diffraction (XRD) and high-resolution transmission electron microscope (HRTEM) were performed to investigate the morphology of ZrO_2. XRD patterns of the ZrO_2 samples were shown in Figure 1a. *m*-ZrO_2 showed characteristic peaks at 28.2°, 31.5°, 34.2°, 49.3° and 50.1° (PDF#37-1484). *t*-ZrO_2 showed characteristic peaks at 30.3°, 35.3°, 50.4°, 50.7°, 59.6°, and 60.2° (PDF#50-1089). The unit cell parameters were calculated for both samples which are in accordance with the PDF cards (see Table S1). The XRD patterns demonstrated that both *m*-ZrO_2 and *t*-ZrO_2 were successfully synthesized. Crystallite sizes of *m*-ZrO_2 and *t*-ZrO_2 were 10.2 nm and 11.7 nm, respectively (see Table 1). The HRTEM images also showed that *m*-ZrO_2 and *t*-ZrO_2 were mainly composed of ~10 nm crystals, which were consistent with the results calculated by Scherrer's equation. The measured interplane spacing of 0.316 nm shown in Figure 1b can be attributed to the $\{\bar{1}11\}$ planes of *m*-ZrO_2, while that of 0.294 nm in Figure 1c can be attributed to {011} lattice planes of *t*-ZrO_2.

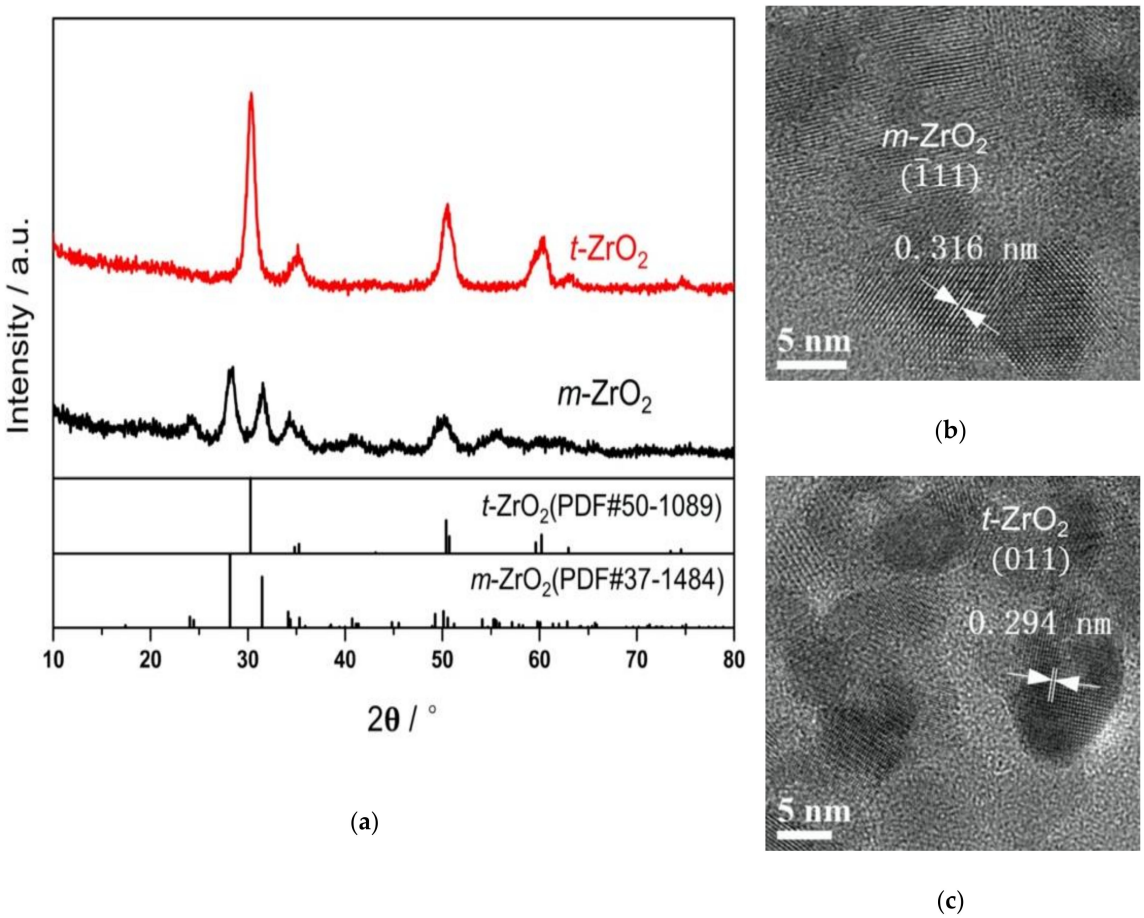

Figure 1. XRD patterns (**a**) and HRTEM images (**b**,**c**) of the ZrO_2 samples.

Table 1. Physical and morphological properties of ZrO_2 samples.

Sample	S_{BET} (m^2/g)	V_{pore} (cm^3/g) [a]	D_{pore} (nm)	Crystallite Size (nm) [b]
m-ZrO_2	60	0.23	15.8	10.2
t-ZrO_2	67	0.33	19.5	11.7

[a] Total pore volume adsorbed at $P/P_0 = 0.99$. [b] Average crystallite size calculated by Scherrer's equation from the peak at $2\theta = 28.2°$ (*m*-ZrO_2) and $2\theta = 30.2°$ (*t*-ZrO_2), respectively.

2.1.2. Interactions of CO with the ZrO_2 Samples

The C–O activation on ZrO_2 samples is a key step in syngas conversion, the adsorption behavior of CO on the surface of ZrO_2 was firstly investigated. The CO-TPD profiles of the ZrO_2 samples are depicted in Figure 2. The desorption peak at around 380 K indicated *m*-ZrO_2 as well as *t*-ZrO_2 had weak interactions with CO molecules. However, two desorption peaks at around 638 K and around 841 K on *m*-ZrO_2 indicated that there were moderate and strong interactions between CO molecules and the surface of *m*-ZrO_2. It can be speculated that more CO molecules can be absorbed on the surface of *m*-ZrO_2 at the reaction temperature (673 K), which are beneficial to C–O activation. Due to the different calcination temperature of samples (773 K for *m*-ZrO_2 and 873 K for *t*-ZrO_2), the peak areas for CO-TPD were calculated from 298 K to 773 K. The results showed that the CO adsorption capacity of *m*-ZrO_2 was 1.6 times higher than that of *t*-ZrO_2. As a result, the CO adsorption studies revealed that *m*-ZrO_2 could adsorb more CO molecules and promote C–O activation.

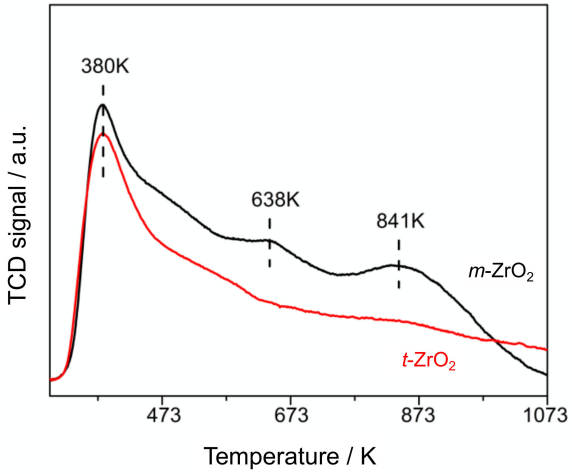

Figure 2. CO-TPD profiles of the ZrO_2 samples.

After CO molecules were absorbed on the surface of ZrO_2 samples, further changes on the catalytic surface were investigated by *in situ* DRIFTs. According to the mechanism of CO activation over ZrO_2 [12], CO molecules are first absorbed on the surface of ZrO_2, then the adsorbed CO molecules react with adjacent hydroxyl groups on the surface and formate species are subsequently formed. Figure 3 shows the DRIFT spectra from 4000 to 2400 cm^{-1}, corresponding to the O–H region and C–H region. Negative peaks at O–H region were observed after introduction of CO and the peak area increased with the time prolonging. This could be attributed to the reaction between the hydroxyl groups and absorbed CO molecules [12]. Two bands of hydroxyl groups at around 3762 cm^{-1} and around 3654 cm^{-1} were observed on *m*-ZrO_2, and hydroxyl groups at around 3762 cm^{-1} and around 3660 cm^{-1} were observed in *t*-ZrO_2 [28]. Meanwhile, formate species were detected on *m*-ZrO_2 (2965 cm^{-1}, 2874 cm^{-1} and 2745 cm^{-1}) and *t*-ZrO_2 (2981 cm^{-1}, 2867 cm^{-1} and 2745 cm^{-1}) [29]. It can be clearly seen that more formate species were formed on the surface of *m*-ZrO_2 than that of *t*-ZrO_2. The integral area of two negative peaks changed over time were calculated and shown in Figure 4a. Apparently, the integral area of *m*-ZrO_2 increased more quickly than that of *t*-ZrO_2 and was nearly twice as large as *t*-ZrO_2 at each moment. Figure 4b showing the consumption rate of –OH indicated that –OH sites on *m*-ZrO_2 were more active than those on *t*-ZrO_2. These results indicate that more CO molecules can interact with the surface hydroxyl groups of *m*-ZrO_2 than that of *t*-ZrO_2, which make *m*-ZrO_2 a better catalyst for C–O activation.

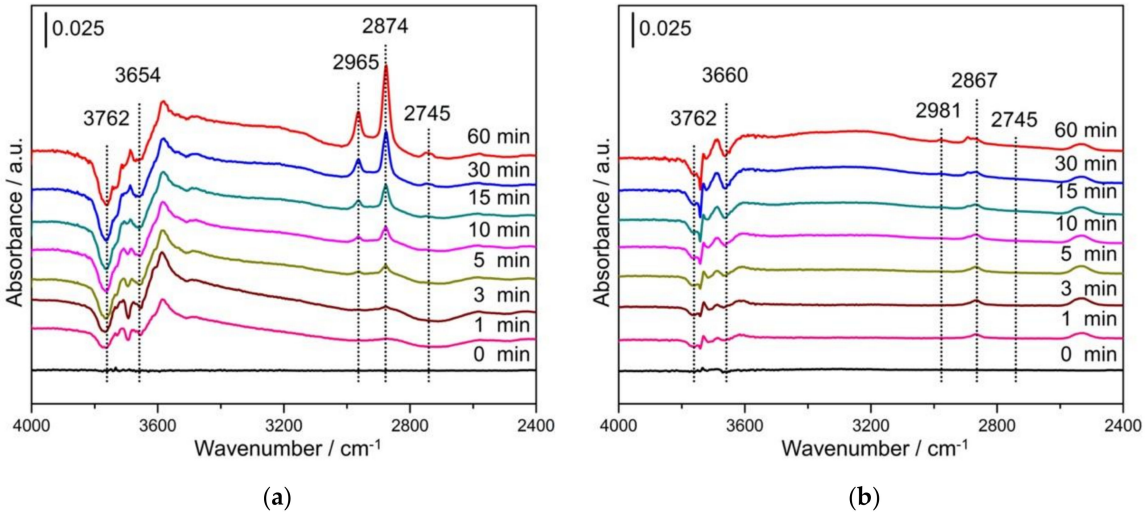

Figure 3. *in situ* DRIFT spectra of the ZrO_2 samples under CO flow. (**a**) *m*-ZrO_2, (**b**) *t*-ZrO_2.

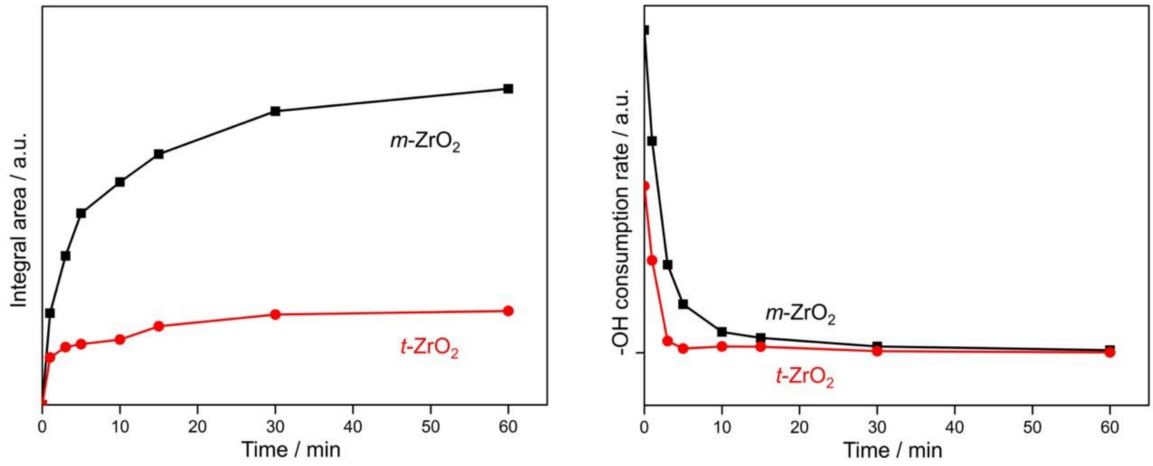

Figure 4. Integral area of –OH peaks (**a**) and the –OH consumption rate (**b**) over the ZrO_2 samples.

2.1.3. Acidity and Basicity Analysis of the ZrO_2 Samples

Usually, the acid and base properties of ZrO_2-based catalysts can significantly affect product distribution in isosynthesis [30]. Therefore, the acidity and basicity of ZrO_2 samples were analyzed by NMR spectroscopy. Trimethylphosphine (TMP) and $^{13}CO_2$ were used as the probe molecules to investigate the acid and base properties of the ZrO_2 samples, respectively [31]. Figure 5a shows the ^{31}P MAS NMR spectra of TMP adsorbed on ZrO_2 samples. ^{31}P signals of adsorbed TMP at around −42 ppm corresponded to Lewis acid sites on the surface of *m*-ZrO_2. There was a broad ^{31}P signal at around 60 ppm, which was assigned to absorbed trimethylphosphine oxide (TMPO) on the Lewis acid sites [32]. Differing from *m*-ZrO_2, two peaks at around −42 ppm and around –29 ppm were found and were assigned to Lewis acid sites on the *t*-ZrO_2 surface [33]. Besides, a ^{31}P signal at –5 ppm assigned to Brønsted acid sites was observed. A quantitative study of Lewis and Brønsted acid sites was shown in Table 2. The total acid content of *m*-ZrO_2 was 217.4 μmol/g compared to 153.5 μmol/g on *t*-ZrO_2, which was similar to the acidity determined by NH_3-TPD (Table S3). The acidic sites on ZrO_2 can promote CO adsorption and activation [34], and therefore *m*-ZrO_2 should have better catalytic performance on C–O activation for syngas conversion due to its high acid density.

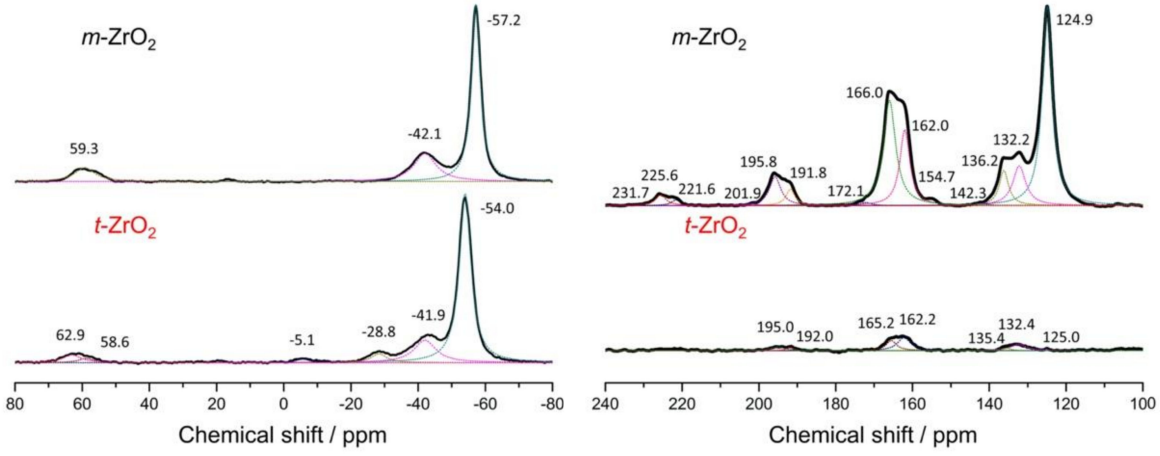

Figure 5. ^{31}P MAS NMR spectra of TMP absorbed on ZrO_2 samples (**a**) and ^{13}C MAS NMR spectra of $^{13}CO_2$ absorbed on ZrO_2 samples (**b**).

Table 2. Acid and base density of the catalysts characterized by the NMR technics [31].

Sample	Acid Density (μmol/g)			Base Density (μmol/g)			
	Lewis Acid	Brønsted Acid	Total	Weak	Moderate	Strong	Total
m-ZrO_2	217.4	-	217.4	49.0	68.1	3.1	120.2
t-ZrO_2	145.2	8.3	153.5	9.1	5.5	-	14.6

Figure 5b presents the ^{13}C MAS NMR spectra of $^{13}CO_2$ adsorbed on ZrO_2 samples. Signal of physisorbed $^{13}CO_2$ is found at around 125 ppm and spinning sideband appeared at around 155 ppm. Three signals at 162, 166, and 172 ppm could be assigned to bidentate bicarbonate species, bidentate carbonate species, and unidentate carbonate species, corresponding to weak, moderate, and strong Lewis basic sites on the ZrO_2 surface, respectively [31]. The respective spinning sidebands were found at 130–145 ppm, 190–203 ppm and 220–232 ppm. Table 2 summarized base density of the ZrO_2 samples, including contributions from the spinning sidebands. The results showed that there were more basic sites on *m*-ZrO_2 than that of *t*-ZrO_2 and the density of total basic sites on *m*-ZrO_2 was 8.2 times higher than that of *t*-ZrO_2. The density of strong Lewis basic sites on *m*-ZrO_2 was 3.1 μmol/g while it was negligible on *t*-ZrO_2. It has been reported that the basic sites of ZrO_2 were favorable for the chain growth reactions [34]. Therefore, the abundant Lewis basic sites on *m*-ZrO_2 due to the coordinative unsaturated Zr^{4+}-O^{2-} pairs can enhance the C–C coupling in syngas conversion reactions.

2.2. Catalytic Performance

The catalytic performance of ZrO_2 and ZrO_2/HZSM-5 catalysts for conversion of syngas was systematically investigated and the results are summarized in Table 3. At 673 K, it is found that the CO conversion was 12.9% on the *m*-ZrO_2 catalyst, which was about 50% more than that of *t*-ZrO_2 catalyst (8.6%). Higher CO conversion could be attributed to higher CO adsorption capacity as well as more active hydroxyl groups on *m*-ZrO_2. As described above, CO molecules were first absorbed on the surface of ZrO_2 samples, and then absorbed CO molecules were reacted with adjacent hydroxyl groups. Our CO-TPD results showed a stronger interaction between the CO molecules and the surface of *m*-ZrO_2 at high temperature. As a result, higher CO conversion could be achieved over *m*-ZrO_2. Similar results were observed at different temperatures, pressure, and gas hourly space velocity (GHSV) (Table S4). Meanwhile, it was found that the selectivity to CH_4 on the *m*-ZrO_2 catalyst was only 5.4%, much lower compared to 29.5% on the *t*-ZrO_2 catalyst, indicating a facilitated C–C coupling on *m*-ZrO_2, which can be attributed to the abundant basic sites on the surface of *m*-ZrO_2 samples.

Table 3. Catalytic results over the ZrO_2 and ZrO_2/HZSM-5 catalysts. [a]

Catalyst	CO Conv. (%)	CO_2 sel. (%)	Product Selectivity (%) [b]				
			CH_4	$C_{2-4}^{=}$	C_{2-4}^{0}	C_{5+}	Ar
m-ZrO_2	12.9	38.3	5.4	57.8	6.7	30.1	-
t-ZrO_2	8.6	36.9	29.5	26.1	19.3	25.1	-
m-ZrO_2/HZSM-5-mix	24.0	36.4	4.3	2.7	21.4	4.2	67.4
t-ZrO_2/HZSM-5-mix	14.2	33.5	4.9	2.6	20.6	6.9	65.0
m-ZrO_2/HZSM-5-db	14.7	41.7	5.8	1.0	66.2	22.1	4.9
t-ZrO_2/HZSM-5-db	8.7	38.5	21.0	1.5	49.5	14.2	13.8

[a] Reaction conditions: 1.50 g for ZrO_2 and 3.00 g for ZrO_2/HZSM-5 (mass ratio = 1:1); H_2/CO = 1:1(volume ratio), F = 25 mL min^{-1}; P = 3.8 MPa, T = 673K, time on stream (TOS) = 8 h. [b] Selectivity in hydrocarbons ($C_{2-4}^{=}$, C_{2-4}^{0}, C_{5+}, and Ar denote C_2–C_4 olefins, C_2–C_4 paraffins, C_{5+} hydrocarbons exclusive of aromatics, and aromatics, respectively).

Bi-functional ZrO_2/HZSM-5 catalysts are known to selectively convert syngas to aromatics [11]. We combined both *m*-ZrO_2 and *t*-ZrO_2 with HZSM-5 (physical and chemical properties of HZSM-5 see Figure S1, Tables S2 and S3) and tested the catalytic performance for the reaction syngas to aromatics (see Table 3). And two types of catalyst loading were adopted for the catalyst evaluation, which are

the single catalyst bed consisted of a blend of ZrO_2 and HZSM-5 samples (denoted as -mix) and the dual bed layered by ZrO_2 and HZMS-5 in sequence (denoted as -db). It is found that the CO conversion was enhanced significantly after *m*-ZrO_2 or *t*-ZrO_2 was combined with HZSM-5 at 673 K. Meanwhile, CH_4 formation was significantly suppressed, especially on the *t*-ZrO_2/HZSM-5-mix catalyst. This phenomenon could be explained by improving the thermodynamic driving force of the reaction due to the rapid removal of intermediates. These intermediates diffuse rapidly into HZSM-5, shifting the chemical equilibrium to the right. It is worth noting that the proximity of the ZrO_2 sample and HZSM-5 were crucial for the diffusion, which was confirmed by dual bed experiments. It can be seen that the CO conversion increased just a little compared to that of ZrO_2 catalysts. Since HZSM-5 was separated by quartz wool, the distance between ZrO_2 and HZSM-5 was too far for intermediates to diffuse into HZSM-5. As a result, the chemical equilibrium remained unchanged. Selectivity to CH_4 was still above 20% on the *t*-ZrO_2/HZSM-5-db catalyst, which meant C_1 intermediates were hydrogenated directly into CH_4 by ZrO_2. Compared to ZrO_2, selectivity to C_2–C_4 olefins on dual bed catalysts decreased while C_2–C_4 paraffins increased, this was due to the hydrogenation ability of HZSM-5. Herein, the combination between ZrO_2 and HZSM-5 is crucial for converting syngas into aromatics. To reduce the distance between the two components and increase the diffusion of the intermediates to HZSM-5, physical mixing was used. After combining ZrO_2 with HZSM-5, the majority of the C_2–C_4 intermediates from the ZrO_2 catalyst can be converted to aromatics over ZrO_2/HZSM-5-mix. The selectivity to C_2–C_4 olefins on both catalysts decreased significantly, and the secondary most products are mainly C_2–C_4 paraffins. The selectivity to aromatics was 67.4% at 673 K over *m*-ZrO_2/HZSM-5-mix catalyst, slightly higher than that of *t*-ZrO_2/HZSM-5-mix catalyst (65.0%). As we are aware, HZSM-5 is widely used to catalyze methanol to aromatics reaction (MTA) for its excellent acidity and pore structure [35]. Intermediates diffused into the channel of HZSM-5 and C–C coupling took place mostly on Brønsted acid sites of HZSM-5 rather than active sites on the ZrO_2. Therefore, the selectivity to aromatics increased significantly. As mentioned above, *m*-ZrO_2 was better at C–C coupling than *t*-ZrO_2, therefore there were more intermediates generated on *m*-ZrO_2, which were essential precursors for aromatization in HZSM-5, which accounted for the superior activity of the *m*-ZrO_2/HZSM-5-mix in the selective conversion of syngas to aromatics.

3. Materials and Methods

3.1. Catalyst Preparation

The *m*-ZrO_2 samples were synthesized by a hydrothermal method [36]. Firstly, $ZrO(NO_3)_2{\cdot}xH_2O$ (7.40 g, 99%, Sigma Aldrich, Shanghai, China) and $CO(NH_2)_2$ (19.22 g, AR, Sinopharm, Shanghai, China) were completely dissolved in deionized water (80 mL) at 298 K under stirring. Then, the solution was transferred to a Teflon-lined stainless-steel autoclave (100 mL) and heated in the oven at 433 K for 20 h. The resulting solids were filtered and washed with deionized water, followed by drying at 373 K overnight and calcination at 773 K for 4 h with a heating rate of 2 K/min.

The *t*-ZrO_2 samples were synthesized via precipitation method [36]. Namely, $ZrOCl_2{\cdot}8H_2O$ (24.17 g, AR, Sinopharm, Shanghai, China) was dissolved in deionized water (150 mL) under stirring, and 50 mL of $NH_3{\cdot}H_2O$ (14.8 M, AR, Sinopharm, Shanghai, China) was added dropwise. Then, the solution was kept at 298 K for 3 h and then heated to 373 K for 48 h under stirring. The precipitates were filtered and washed with deionized water, which was followed by drying at 383 K overnight and calcination at 873 K for 5 h with a heating rate of 10 K/min.

The ZrO_2/HZSM-5 bi-functional catalysts were prepared via a physical mixing method. The two components ZrO_2 and HZSM-5 (Si/Al molar ratio = 120, Nankai University Catalyst Co., Ltd., Tianjin, China) were mixed and grinded in an agate mortar for 30 min.

3.2. Catalyst Characterization

The XRD patterns were obtained using a Bruker D8 X-ray diffractometer (Bruker, Karlsruhe, Germany) with a position sensitive detector (PSD) detector and Cu K α radiation (40 kV, 40 mA) with 2θ range of 10-80°. HRTEM images were obtained by a JEOL JEM-2001 microscope (JEOL, Tokyo, Japan) at 200 kV. The BET surface areas were measured by N_2 physisorption at 77 K on a Quadrasorb Evo apparatus (Quantachrome, Ashland, VA, America). Prior to the measurements, all samples were treated at 523 K for 3 h under vacuum conditions. CO-TPD was measured on a Micromeritics Autochem II 2920 apparatus (Micromeritics, Norcross, GA, America) equipped with a thermal conductivity detector (TCD) detector. Typically, a 100 mg sample was reduced in 10% H_2/Ar at 773 K for 90 min, following by cooling to room temperature under He flow. Pure CO was then introduced at 298 K for 30 min. After purging by He flow for 30 min, the sample was heated to 1073 K at a heating rate of 10 K/min. *in situ* DRIFTs were performed on a Nicolet 6700 instrument (ThermoFisher, Waltham, MA, America). Before the measurement, catalyst was pretreated with 2% H_2/He flow at 773 K for 1 h. Subsequently, the catalyst was cooled down to 553 K in He atmosphere. The spectra were obtained by collecting 120 scans at 4 cm^{-1} resolution after 5% CO/He being introduced with background collecting under the same condition in He flow. ^{31}P MAS NMR experiments were performed on a Bruker AVANCE III 400 WB spectrometer (Bruker, Wormer, Switzerland) operating at a ^{31}P frequency of 162.1 MHz. ^{13}C MAS NMR measurement were performed on the same Bruker AVANCE III 400 WB spectrometer (Bruker, Wormer, Switzerland) operating at a ^{13}C frequency of 100.7 MHz. NH_3-TPD was measured on a Micromeritics Autochem II 2920 apparatus (Micromeritics, Norcross, GA, America) equipped with a TCD detector.

3.3. Catalytic Reaction

Conversion of syngas was performed on an automated continuous fixed-bed reactor with a stainless-steel reactor lined with a quartz tube (inner diameter = 6 mm) as described before [13]. Typically, 1.5 g catalyst (40–60 mesh) for ZrO_2 or 3.0 g catalyst (40–60 mesh) for ZrO_2/HZSM-5 with the mass ratio = 1/1 was packed in the center of reactor. Normally, the ZrO_2 samples were mixed with HZSM-5 thoroughly and marked with -mix. In dual bed experiments, HZSM-5 was packed below ZrO_2 samples, separated by an inert layer of quartz wool and mark with -db. The catalyst was pretreated in H_2 at 773 K for 1 h before the reaction. The flow rate of syngas (H_2/CO/Ar = 48/48/4, volume ratio) was 25 mL/min (STP), and the reaction pressure was set to 3.8 MPa. The reaction temperature was 673 K and TOS was 8 h.

The permanent gases were analyzed by GC-9160 (Shanghai Sailuxin Analysis Technology Co., Ltd., Shanghai, China) equipped with a thermal conductivity detector (TCD) connected to a 13X molecular sieves packed column (2 m × 3 mm × 2 mm) with a pre-linked Porapak Q (2 m × 3 mm × 2 mm), while aromatics and other hydrocarbons were analyzed on-line by Trace GC Ultra (ThermoFisher, Shanghai, China) equipped with a flame ionization detectors (FID) connected to a AT-PEG-20M capillary column (30 m × 0.32 mm × 0.50μm) and GC-9160 equipped with a flame ionization detectors (FID) connected to a CP-PoraPLOT Q capillary column (50 m × 0.32 mm × 10μm), respectively.

The hydrocarbon products of the reaction are classified into CH_4, C_2–C_4 olefins, C_2–C_4 paraffins, C_{5+} hydrocarbons exclusive of aromatics (consisted of paraffinic and mostly C_5 hydrocarbon), and aromatics (included BTX and C_{9+} aromatics such as trimethylbenzene), which was denoted as CH_4, $C_{2-4}{}^{=}$, $C_{2-4}{}^{0}$, C_{5+} and Ar, respectively.

CO conversion was calculated as:

$$\text{Conversion(CO)} = \frac{CO_{in} - CO_{out}}{CO_{in}} \times 100\%$$

CO_2 selectivity was calculated as:

$$\text{Selectivity}(CO_2) = \frac{CO_{2,\,out}}{CO_{in} - CO_{out}} \times 100\%$$

The selectivity of individual hydrocarbon based on hydrocarbon was calculated as:

$$\text{Selectivity}\left(C_iH_j\right) = \frac{i\,C_iH_{j,\,out}}{\sum_1^n i\,C_iH_{j,\,out}} \times 100\%$$

The carbon balance is about 95%.

4. Conclusions

In this work, the crystalline phases of ZrO_2 significantly influence the activity for syngas conversion to form hydrocarbon intermediates, *m*-ZrO_2 exhibits higher conversion of CO with a higher selectivity to C_{2+} hydrocarbons. The surface of *m*-ZrO_2 contains more hydroxyl groups which react with CO into formate species, and these are crucial for the activation of C–O. NMR results reveal that there are more acid and basic sites existing on *m*-ZrO_2, which exhibits higher activity for C–C coupling. Both CO conversion, as well as the selectivity of aromatic hydrocarbons, can be enhanced after the combination of ZrO_2 with HZSM-5, and *m*-ZrO_2/HZSM-5-mix exhibits superior activity for the selective conversion of syngas to aromatics with less CH_4.

Supplementary Materials: The following are available online at http://www.mdpi.com/2073-4344/10/2/262/s1, Figure S1: XRD patterns of the HZSM-5 zeolite, Table S1: Unit cell parameters for ZrO_2 samples, Table S2: Physical and morphological properties of HZSM-5, Table S3: NH_3-TPD data of ZrO_2 samples and HZSM-5 zeolite, Table S4: Catalytic results over the ZrO_2 and ZrO_2/HZSM-5 catalysts.

Author Contributions: S.W., Z.H. conceived and designed the experiments; S.W. and Y.F. performed the experiments; S.W. analyzed the data and wrote the paper; H.X. and W.S. revised the paper. All authors have read and agreed to the published version of the manuscript.

Funding: This research was funded by the National Key R&D Program of Ministry of Science and Technology (Grant No. 2017YFB0602204), National Natural Science Foundation of China (Grant No. 91645201) and the Shanghai Science and Technology Committee (Grant No. 14DZ2273900).

Conflicts of Interest: The authors declare no conflict of interest.

References

1. Niziolek, A.M.; Onel, O.; Guzman, Y.A.; Floudas, C.A. Biomass-Based production of benzene, toluene, and xylenes via methanol: Process synthesis and deterministic global optimization. *Energy Fuels* **2016**, *30*, 4970–4998. [CrossRef]
2. Torres Galvis, H.M.; de Jong, K.P. Catalysts for production of lower olefins from synthesis gas: A review. *ACS Catal.* **2013**, *3*, 2130–2149. [CrossRef]
3. Olsbye, U.; Svelle, S.; Bjorgen, M.; Beato, P.; Janssens, T.V.; Joensen, F.; Bordiga, S.; Lillerud, K.P. Conversion of methanol to hydrocarbons: How zeolite cavity and pore size controls product selectivity. *Angew. Chem. Int. Ed.* **2012**, *51*, 5810–5831. [CrossRef] [PubMed]
4. Kasipandi, S.; Bae, J.W. Recent advances in direct synthesis of value-added aromatic chemicals from syngas by cascade reactions over bifunctional catalysts. *Adv. Mater.* **2019**, *31*, 1803390. [CrossRef] [PubMed]
5. Lu, Y.; Hu, J.; Han, J.; Yu, F. Synthesis of gasoline-Range hydrocarbons from nitrogen-Rich syngas over a Mo/HZSM-5 bi-functional catalyst. *J. Energy Inst.* **2016**, *89*, 782–792. [CrossRef]
6. Kang, J.; Wang, X.; Peng, X.; Yang, Y.; Cheng, K.; Zhang, Q.; Wang, Y. Mesoporous zeolite Y-Supported Co nanoparticles as efficient Fischer−Tropsch catalysts for selective synthesis of diesel fuel. *Ind. Eng. Chem. Res.* **2016**, *55*, 13008–13019. [CrossRef]
7. Wang, C.; Xu, L.; Wang, Q. Review of directly producing light olefins via CO hydrogenation. *J. Nat. Gas Chem.* **2003**, *12*, 10–16.

8. Jiao, F.; Li, J.; Pan, X.; Xiao, J.; Li, H.; Ma, H.; Wei, M.; Pan, Y.; Zhou, Z.; Li, M.; et al. Selective conversion of syngas to light olefins. *Science* **2016**, *351*, 1065–1068. [CrossRef]
9. Cheng, K.; Gu, B.; Liu, X.; Kang, J.; Zhang, Q.; Wang, Y. Direct and highly selective conversion of synthesis gas into lower olefins: Design of a bifunctional catalyst combining methanol synthesis and carbon–Carbon coupling. *Angew. Chem. Int. Ed.* **2016**, *55*, 4725–4728. [CrossRef]
10. Yang, J.; Pan, X.; Jiao, F.; Li, J.; Bao, X. Direct conversion of syngas to aromatics. *Chem. Commun.* **2017**, *53*, 11146–11149. [CrossRef]
11. Cheng, K.; Zhou, W.; Kang, J.; He, S.; Shi, S.; Zhang, Q.; Pan, Y.; Wen, W.; Wang, Y. Bifunctional catalysts for one-step conversion of syngas into aromatics with excellent selectivity and stability. *Chem* **2017**, *3*, 334–347. [CrossRef]
12. Liu, X.; Zhou, W.; Yang, Y.; Cheng, K.; Kang, J.; Zhang, L.; Zhang, G.; Min, X.; Zhang, Q.; Wang, Y. Design of efficient bifunctional catalysts for direct conversion of syngas into lower olefins via methanol/dimethyl ether intermediates. *Chem. Sci.* **2018**, *9*, 4708–4718. [CrossRef] [PubMed]
13. Huang, Z.; Wang, S.; Qin, F.; Huang, L.; Yue, Y.; Hua, W.; Qiao, M.; He, H.; Shen, W.; Xu, H. Ceria-Zirconia/zeolite bifunctional catalyst for highly selective conversion of syngas into aromatics. *ChemCatChem* **2018**, *10*, 4519–4524. [CrossRef]
14. Zhou, W.; Shi, S.; Wang, Y.; Zhang, L.; Wang, Y.; Zhang, G.; Min, X.; Cheng, K.; Zhang, Q.; Kang, J.; et al. Selective conversion of syngas to aromatics over a Mo-ZrO_2/H-ZSM-5 bifunctional catalyst. *ChemCatChem* **2019**, *11*, 1681–1688. [CrossRef]
15. Liu, J.; He, Y.; Yan, L.; Li, K.; Zhang, C.; Xiang, H.; Wen, X.; Li, Y. Nano-Sized ZrO_2 derived from metal–Organic frameworks and their catalytic performance for aromatic synthesis from syngas. *Catal. Sci. Technol.* **2019**, *9*, 2982–2992. [CrossRef]
16. Xu, H.; Li, M.; Nawaz, M.A.; Liu, D. Doping of K and Zn elements in FeZr-Ni/ZSM-5: Highly selective catalyst for syngas to aromatics. *Catal. Commun.* **2019**, *121*, 95–99. [CrossRef]
17. Xu, Y.; Liu, J.; Wang, J.; Ma, G.; Lin, J.; Yang, Y.; Li, Y.; Zhang, C.; Ding, M. Selective conversion of syngas to aromatics over Fe_3O_4@MnO_2 and hollow HZSM-5 bifunctional catalysts. *ACS Catal.* **2019**, *9*, 5147–5156. [CrossRef]
18. Pokrovski, K.; Jung, K.T.; Bell, A.T. Investigation of CO and CO_2 adsorption on tetragonal and monoclinic zirconia. *Langmuir* **2001**, *17*, 4297–4303. [CrossRef]
19. Fan, Y.; Cheng, S.; Wang, H.; Tian, J.; Xie, S.; Pei, Y.; Qiao, M.; Zong, B. Pt–WO_x on monoclinic or tetrahedral ZrO_2: Crystal phase effect of zirconia on glycerol hydrogenolysis to 1,3-Propanediol. *Appl. Catal. B Environ.* **2017**, *217*, 331–341. [CrossRef]
20. Liu, S.; Wang, H.; Wei, Y.; Zhang, R.; Royer, S. Morphology-Oriented ZrO_2-supported vanadium oxide for the NH_3-SCR process: Importance of structural and textural properties. *ACS Appl. Mater. Interfaces* **2019**, *11*, 22240–22254. [CrossRef]
21. Foraita, S.; Fulton, J.L.; Chase, Z.A.; Vjunov, A.; Xu, P.; Barath, E.; Camaioni, D.M.; Zhao, C.; Lercher, J.A. Impact of the oxygen defects and the hydrogen concentration on the surface of tetragonal and monoclinic ZrO_2 on the reduction rates of stearic acid on Ni/ZrO_2. *Chem. Eur. J.* **2015**, *21*, 2423–2434. [CrossRef] [PubMed]
22. De Souza, P.M.; Rabelo-Neto, R.C.; Borges, L.E.P.; Jacobs, G.; Davis, B.H.; Graham, U.M.; Resasco, D.E.; Noronha, F.B. Effect of zirconia morphology on hydrodeoxygenation of phenol over Pd/ZrO_2. *ACS Catal.* **2015**, *5*, 7385–7398. [CrossRef]
23. Gu, H.; Ding, J.; Zhong, Q.; Zeng, Y.; Song, F. Promotion of surface oxygen vacancies on the light olefins synthesis from catalytic CO_2 hydrogenation over Fe-K/ZrO_2 catalysts. *Int. J. Hydrog. Energ.* **2019**, *44*, 11808–11816. [CrossRef]
24. Maruya, K.-I.; Komiya, T.; Hayakawa, T.; Lu, L.; Yashima, M. Active sites on ZrO_2 for the formation of isobutene from CO and H_2. *J. Mol. Catal. A Chem.* **2000**, *159*, 97–102. [CrossRef]
25. Witoon, T.; Chalorngtham, J.; Dumrongbunditkul, P.; Chareonpanich, M.; Limtrakul, J. CO_2 hydrogenation to methanol over Cu/ZrO_2 catalysts: Effects of zirconia phases. *Chem. Eng. J.* **2016**, *293*, 327–336. [CrossRef]
26. Ma, Z.-Y.; Yang, C.; Wei, W.; Li, W.-H.; Sun, Y.-H. Catalytic performance of copper supported on zirconia polymorphs for CO hydrogenation. *J. Mol. Catal. A Chem.* **2005**, *231*, 75–81. [CrossRef]
27. He, D.; Ding, Y.; Luo, H.; Li, C. Effects of zirconia phase on the synthesis of higher alcohols over zirconia and modified zirconia. *J. Mol. Catal. A Chem.* **2004**, *208*, 267–271. [CrossRef]

28. Bachiller-Baeza, B.; Rodriguez-Ramos, I.; Guerrero-Ruiz, A. Interaction of carbon dioxide with the surface of zirconia polymorphs. *Langmuir* **1998**, *14*, 3556–3564. [CrossRef]
29. Wu, X.; Tan, M.; Tian, S.; Song, F.; Ma, Q.; He, Y.; Yang, G.; Tsubaki, N.; Tan, Y. Designing ZrO_2-Based catalysts for the direct synthesis of isobutene from syngas: The studies on Zn promoter role. *Fuel* **2019**, *243*, 34–40. [CrossRef]
30. Li, Y.; He, D.; Zhu, Q.; Zhang, X.; Xu, B. Effects of redox properties and acid–Base properties on isosynthesis over ZrO_2-Based catalysts. *J. Catal.* **2004**, *221*, 584–593. [CrossRef]
31. Fu, Y.; Zhang, L.; Yue, B.; Chen, X.; He, H. Simultaneous characterization of solid acidity and basicity of metal oxide catalysts via the solid-state NMR technique. *J. Phys. Chem. C* **2018**, *122*, 24094–24102. [CrossRef]
32. Zheng, A.; Huang, S.-J.; Liu, S.-B.; Deng, F. Acid properties of solid acid catalysts characterized by solid-state ^{31}P NMR of adsorbed phosphorous probe molecules. *Phys. Chem. Chem. Phys.* **2011**, *13*, 14889–14901. [CrossRef] [PubMed]
33. Shimizu, K.; Venkatraman, T.; Song, W. NMR study of tungstated zirconia catalyst: Acidic properties of tungstated zirconia and influence of tungsten loading. *Appl. Catal. A Gen.* **2002**, *224*, 77–87. [CrossRef]
34. Li, Y.; He, D.; Yuan, Y.; Cheng, Z.; Zhu, Q. Selective formation of isobutene from CO hydrogenation over zirconium dioxide based catalysts. *Energy Fuels* **2001**, *15*, 1434–1440. [CrossRef]
35. Stöcker, M. Methanol-To-Hydrocarbons: Catalytic materials and their behavior. *Micropor. Mesopor. Mater.* **1999**, *29*, 3–48. [CrossRef]
36. Li, W.; Huang, H.; Li, H.; Zhang, W.; Liu, H. Facile synthesis of pure monoclinic and tetragonal zirconia nanoparticles and their phase effects on the behavior of supported molybdena catalysts for methanol-Selective oxidation. *Langmuir* **2008**, *24*, 8358–8366. [CrossRef]